J Biol Inorg Chem (2014) 19:335–348
DOI 10.1007/s00775-013-1069-2

ORIGINAL PAPER

Mitochondria are the primary target in the induction of apoptosis by chiral ruthenium(II) polypyridyl complexes in cancer cells

Jin-Quan Wang · Ping-Yu Zhang · Chen Qian · Xiao-Juan Hou · Liang-Nian Ji · Hui Chao

Received: 11 September 2013 / Accepted: 12 November 2013 / Published online: 28 November 2013

Abstract A series of novel chiral ruthenium(II) polypyridyl complexes (**Δ-Ru1, Λ-Ru1, Δ-Ru2, Λ-Ru2, Δ-Ru3, Λ-Ru3**) were synthesized and evaluated to determine their antiproliferative activities. Colocalization, inductively coupled plasma mass spectrometry, and 3-(4,5-dimethylthiazol-2-yl)-2,5-diphenyltetrazolium bromide assay studies showed that these ruthenium(II) complexes accumulated preferentially in the mitochondria and exhibited cytotoxicity against various cancer cells in vitro. The complex **Δ-Ru1** is of particular interest because it was found to have half-maximal inhibitory concentrations comparable to those of cisplatin and better activity than cisplatin against a cisplatin-resistant cell line, A549-CP/R. **Δ-Ru1** induced alterations in the mitochondrial membrane potential and triggered intrinsic mitochondria-mediated apoptosis in HeLa cells, which involved the regulation of Bcl-2 family members and the activation of caspases. Taken together, these data suggest that **Δ-Ru1** may be a novel mitochondria-targeting anticancer agent.

Keywords Ruthenium(II) complexes · Mitochondria targeting · Cytotoxicity · Apoptosis

Introduction

Although cisplatin is active against a variety of cancers, its use is often associated with severe dose-limiting side effects, including nephrotoxicity, neurotoxicity, and gastrointestinal toxicity [1–4]. In addition, other factors, such as low water solubility and drug resistance, have limited the clinical applications of cisplatin [5, 6]. These limitations have led to an urgent search for other metal-based agents that can replace platinum-based drugs. In recent years, ruthenium-based complexes have emerged as promising antitumor and antimetastatic agents with equal or even greater antitumor activity and lower toxicity [7, 8]. To date, two ruthenium-based complexes, NAMI-A and KP1019, have entered human clinical trials [9, 10]. These two ruthenium(III) complexes exhibited great antitumor activity in preclinical studies. NAMI-A had inhibitory effects against the formation of cancer metastases in a variety of animal models but lacked direct cytotoxic effects on the primary tumor [11]. In contrast, KP1019 exhibited direct antitumor effects against a series of primary human tumor explants [12]. In addition, several mechanisms have been proposed to explain the anticancer effects of these ruthenium complexes, including interaction with DNA [13–16], modification of the cell membrane and cell adhesion properties [17], blocking of the cell cycle [18], and inhibition of various kinases [19] and topoisomerase [20–22].

Electronic supplementary material The online version of this article (doi:10.1007/s00775-013-1069-2) contains supplementary material, which is available to authorized users.

J.-Q. Wang · P.-Y. Zhang · C. Qian · L.-N. Ji · H. Chao (✉)
MOE Key Laboratory of Bioinorganic and Synthetic Chemistry, State Key Laboratory of Optoelectronic Materials and Technologies, School of Chemistry and Chemical Engineering, Sun Yat-Sen University, Guangzhou 510275, People's Republic of China
e-mail: ceschh@mail.sysu.edu.cn

J.-Q. Wang
Guangdong Pharmaceutical University, Guangzhou 510006, People's Republic of China

X.-J. Hou
Huaihua Medical College, Huaihua 418000, People's Republic of China

Recently, a novel chemotherapeutic mechanism involving the disruption of mitochondria has been investigated because this mechanism circumvents upstream apoptotic pathways that may be mutated or lacking in cancer cells [23]. Cancer cell mitochondria are structurally and functionally different from their normal counterparts. Accordingly, tumor cells often use glycolysis for ATP generation, which is normally performed primarily by oxidative phosphorylation [24]. Moreover, cancer cells have higher mitochondrial membrane potentials, rendering them more susceptible to mitochondrial perturbations than nonimmortalized cells. On the basis of these factors, dozens of mitochondria-targeting agents have emerged as a means to disrupt the mitochondrial membrane potential and further permeabilize the mitochondrial outer membrane, leading to the release of proapoptotic proteins and the impairment of the bioenergetic functions of mitochondria [25]. The activation of the cell death machinery in cancer cells by inhibiting tumor-specific alterations to mitochondrial metabolism or by stimulating mitochondrial membrane permeabilization could therefore be a promising strategy in cancer therapy [26].

It has been reported that some ruthenium(II) complexes, especially those bearing 2-phenylimidazo[4,5-*f*][1,10]phenanthroline (PIP) ligands, can induce mitochondria -mediated apoptosis in cancer cells [27–36]. Motivated by these findings, we synthesized six chiral ruthenium polypyridyl complexes (**Δ-Ru1**, **Λ-Ru1**, **Δ-Ru2**, **Λ-Ru2**, **Δ-Ru3**, and **Λ-Ru3**, as shown in Fig. 1). To explore the structure–activity relationship of ruthenium(II) complexes, we functionalized PIP by replacing one benzene ring with another heterocycle with a hydroxyl group, in which an *ortho* hydroxyl group that may form an intramolecular hydrogen bond with the nitrogen atom of the imidazole ring was introduced into the ligands to extend the planarity. Inductively coupled plasma mass spectrometry (ICP-MS) showed that these six complexes accumulated primarily in the mitochondria. When comparing these six complexes, we found that the cytotoxicity was correlated with the cellular uptake properties, and **Δ-Ru1** exhibited the highest cytotoxicity. Further investigations, including live-cell imaging, transmission electron microscopy, flow cytometry, and Western blot analysis, demonstrated that the mitochondria are the primary target of **Δ-Ru1** in the induction of apoptosis in cancer cells.

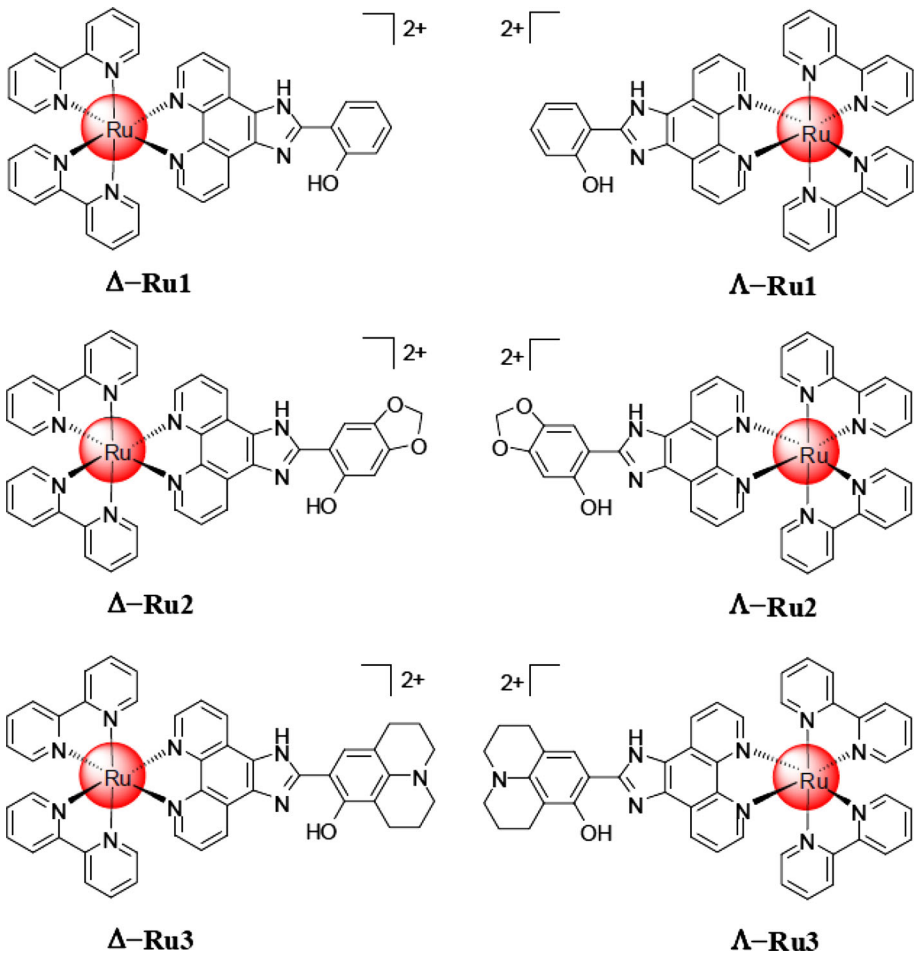

Fig. 1 Chemical structures of the ruthenium(II) complexes studied

Materials and methods

Materials

All reagents and solvents were of analytical grade unless otherwise noted. Cisplatin, 4′,6-diamino-2-phenylindole (DAPI), 2′,7′-dichlorofluorescein diacetate (DCFH-DA), and 3-(4,5-dimethylthiazol-2-yl)-2,5-diphenyltetrazolium bromide (MTT) were obtained from Sigma-Aldrich. Stock solutions of cisplatin (10 mM) and ruthenium(II) complexes (1 mM) were prepared in dimethyl sulfoxide (DMSO), and were stable for at least 48 h at room temperature, as monitored by UV–visible spectroscopy. 1,10-Phenanthroline-5,6-dione [37], Δ-[Ru(bpy)$_2$(py)$_2$][*O*,*O*′-dibenzoyl-D-tartrate]·12H$_2$O [38] (where bpy is 2,2′-bipyridyl and py is pyridyl), and Λ-[Ru(bpy)$_2$(py)$_2$] [*O*,*O*′-dibenzoyl-D-tartrate]·12H$_2$O [38] were prepared according to methods described in the literature.

Syntheses

2-(2-Hydroxyphenyl)imidazo[4,5-f][1,10]phenanthroline

2-(2-Hydroxyphenyl)imidazo[4,5-*f*][1,10]phenanthroline (HPIP) was prepared according to methods described in the literature [15]. Anal. Calcd for $C_{19}H_{12}N_4O$ (%): C, 73.07; H, 3.87; N, 17.94. Found (%): C, 73.05; H, 3.90; N, 17.91. ^{1}H NMR (400 MHz, DMSO-d_6): δ (ppm) 8.84 (d, $J = 7.8$ Hz, 2H), 8.24 (d, $J = 7.6$ Hz, 2H), 7.74 (dd, $J = 6.9$ Hz, 1H), 7.49 (t, $J = 6.9$ Hz, 2H) 7.42 (t, $J = 6.9$ Hz, 1H), 7.26 (t, $J = 6.9$ Hz, 1H), 7.20 (d, $J = 6.9$ Hz, 1H). Fast atom bombardment mass spectrometry (FAB-MS): *m*/*z* 313 (M + 1).

2-(6-Hydroxy-3,4-methylenedioxyphenyl)imidazo[4,5-f][1,10]-phenanthroline

A mixture of 1,10-phenanthroline-5,6-dione (0.21 g, 1 mmol), 6-hydroxy-3,4-(methylenedioxy)benzaldehyde (0.166 g, 1 mmol), ammonium acetate (1.94 g, 25.0 mmol), and glacial acetic acid (15 mL) was refluxed with stirring for 4 h. The yellow-brown precipitate was removed by filtration while hot, washed with H$_2$O and diethyl ether, and then dried in vacuo. The resulting crude solid was purified by chromatography over 100-mesh SiO$_2$ using ethanol as the eluent and then dried in vacuo to afford 2-(6-hydroxy-3,4-methylenedioxyphenyl)imidazo[4,5-*f*][1,10]-phenanthroline (HMIP). Yield: 0.30 g (84.2 %). Anal. Calcd for $C_{20}H_{12}N_4O_3$ (%): C, 67.42; H, 3.39; N, 15.72. Found (%): C, 67.45; H, 3.36; N, 15.74. ^{1}H NMR (400 MHz, DMSO-d_6): δ (ppm) 8.87 (d, $J = 7.8$ Hz, 2H), 8.14 (d, $J = 7.5$ Hz, 2H), 7.39 (dd, $J = 8.0$ Hz, 2H), 7.12 (s, 1H), 6.61 (s, 1H), 6.06 (s, 2H). FAB-MS: *m*/*z* 357 (M + 1).

2-(8-Hydroxyjulodinyl)imidazo[4,5-f][1,10]phenanthroline

A mixture of 1,10-phenanthroline-5,6-dione (0.21 g, 1 mmol), 9-formyl-8-hydroxyjulodine (0.217 g, 1 mmol), ammonium acetate (1.94 g, 25.0 mmol), and glacial acetic acid (15 mL) was refluxed with stirring for 4 h. The yellow-brown precipitate was removed by filtration while hot, washed with H$_2$O and diethyl ether, and then dried in vacuo. The resulting crude solid was purified by chromatography over 100-mesh SiO$_2$ using ethanol as the eluent and then dried in vacuo to afford 2-(8-hydroxyjulodinyl)imidazo[4,5-*f*][1,10]phenanthroline (HQIP). Yield: 0.35 g (85.9 %). Anal. Calcd for $C_{25}H_{21}N_5O$ (%): C, 73.69; H, 5.19; N, 17.19. Found (%): C, 73.66; H, 5.21; N, 17.21. ^{1}H NMR (400 MHz, DMSO-d_6): δ (ppm) 8.90 (dd, $J = 7.8$ Hz, 2H), 8.24 (dd, $J = 7.5$ Hz, 2H), 7.48 (m, 3H), 3.37 (t, $J = 7.3$ Hz, 4H), 2.97 (t, $J = 7.7$ Hz, 2H), 2.79 (t, $J = 7.7$ Hz, 2H), 1.96 (m, 4H). FAB-MS: *m*/*z* 408 (M + 1).

Δ-Ru1

Δ-[Ru(bpy)$_2$(HPIP)](ClO$_4$)$_2$ (**Δ-Ru1**) was prepared according to methods described in the literature [15]. Anal. Calcd for $C_{39}H_{28}N_8ORu$ (%): C, 64.54; H, 3.89; N, 15.44. Found (%): C, 64.51; H, 3.92; N, 15.43. ^{1}H NMR (400 MHz, DMSO-d_6): δ (ppm) 9.14 (d, $J = 8.2$ Hz, 2H), 8.86 (d, $J = 8.2$ Hz, 2H), 8.86 (d, $J = 8.2$ Hz, 2H), 8.20 (t, $J = 8.4$ Hz, 2H), 8.02–8.13 (m, 4H), 7.88–7.93 (m, 2H), 7.83 (*d*, J = 5.2 Hz, 2H), 7.58 (dd, $J = 7.4$ Hz, 4H), 7.42 (t, $J = 8.2$ Hz, 2H), 7.32 (t, $J = 8.0$ Hz, 2H), 7.09 (t, $J = 7.8$ Hz, 2H). Electrospray mass spectrometry (ES-MS) (CH_3CN): *m*/*z* 726 ([M − 2ClO$_4$ + H]$^+$), 363 ([M − 2ClO$_4$]$^{2+}$). Circular dichroism (CD) (H$_2$O): λ/nm ($\Delta\varepsilon$/M^{-1} cm^{-1}) 472 (−10.7), 421 (9.7), 291 (−116.8), 274 (34.6), 240 (15.9).

Λ-Ru1

Λ-[Ru(bpy)$_2$(HPIP)](ClO$_4$)$_2$ (**Λ-Ru1**) was prepared according to methods described in the literature [15]. The elemental analysis, ^{1}H NMR, and mass spectral data for **Λ-Ru1** were the same as those for **Δ-Ru1**, within experimental error. CD (H$_2$O): λ/nm ($\Delta\varepsilon$/M^{-1} cm^{-1}) 472 (10.8), 421 (-9.8), 291 (117.0), 274 (−35.1), 240 (−15.8).

Δ-Ru2

A mixture of Δ-[Ru(bpy)$_2$(py)$_2$][*O*,*O*′-dibenzoyl-D-tartrate]·12H$_2$O (0.2 g, 0.2 mmol), HMIP (0.071 g, 0.2 mmol),

and ethylene glycol (10 mL) was refluxed under argon for 8 h, and the color of the solution changed from purple to red. The solution was cooled to room temperature, and 20 mL of H_2O was added. After filtration, a dark-red precipitate was obtained by the dropwise addition of an aqueous $NaClO_4$ solution. The crude product was purified by column chromatography using neutral alumina with CH_3CN–toluene (4:1, v/v) as the eluent. The red-brown band was collected. The solvent was removed under reduced pressure, and Δ-[Ru(bpy)$_2$(HMIP)](ClO$_4$)$_2$ (**Δ-Ru2**) was obtained as a red-brown powder. Yield: 0.17 g (87.6 %). Anal. Calcd for $C_{40}H_{28}N_8O_3Ru$ (%): C, 62.41; H, 3.67; N, 14.56. Found (%): C, 62.43; H, 3.69; N, 14.55. ^{1}H NMR (400 MHz, DMSO-d_6): δ (ppm) 9.08 (d, $J = 8.0$ Hz, 2H), 8.84 (dd, $J = 8.2$ Hz, 4H), 8.20 (t, $J = 7.9$ Hz, 2H), 8.08 (dd, $J = 7.9$ Hz, 4H), 7.91 (d, $J = 7.8$ Hz, 2H), 7.82 (d, $J = 8.3$ Hz, 2H), 7.69 (s, 1H), 7.57 (m, 4H), 7.32 (t, $J = 7.8$ Hz, 2H), 6.74 (s, 1H), 6.09 (s, 2H). ES-MS (CH_3CN): *m/z* 770 ([M − 2ClO$_4$ + H]$^+$), 384 ([M − 2ClO$_4$]$^{2+}$). CD (H_2O): λ/nm ($\Delta\varepsilon$/M^{-1} cm^{-1}) 471 (−13.6), 420 (14.3), 291 (−169.8), 274 (59.4), 240 (18.8).

Λ-Ru2

Λ-[Ru(bpy)$_2$(HMIP)](ClO$_4$)$_2$ (**Λ-Ru2**) was synthesized in a manner identical to that described for **Δ-Ru2**, but using Λ-[Ru(bpy)$_2$(py)$_2$][*O*,*O*′-dibenzoyl-L-tartrate]·12H$_2$O (0.20 g, 0.2 mmol) rather than Δ-[Ru(bpy)$_2$(py)$_2$][*O*,*O*′-dibenzoyl-D-tartrate]·12H$_2$O. Yield: 0.16 g (85.6 %). The elemental analysis, ^{1}H NMR, and mass spectral data for **Λ-Ru2** were the same as those for **Δ-Ru2**, within experimental error. CD (H_2O): [λ/nm ($\Delta\varepsilon$/M^{-1} cm^{-1}) 471 (13.9), 420 (−14.5), 291 (171.0), 274 (−59.9), 240 (−19.0).

Δ-Ru3

A mixture of Δ-[Ru(bpy)$_2$(py)$_2$][*O*,*O*′-dibenzoyl-D-tartrate]·12H$_2$O (0.2 g, 0.2 mmol), HQIP (0.081 g, 0.2 mmol), and ethylene glycol (10 mL) was refluxed under argon for 8 h, and the color of the solution changed from purple to red. The solution was cooled to room temperature, and 20 mL of H_2O was added. After filtration, a dark-red precipitate was obtained by the dropwise addition of an aqueous $NaClO_4$ solution. The crude product was purified by column chromatography using neutral alumina with CH_3CN–toluene (4:1, v/v) as the eluent. The red-brown band was collected. The solvent was removed under reduced pressure, and Δ-[Ru(bpy)$_2$(HQIP)](ClO$_4$)$_2$ (**Δ-Ru3**) was obtained as a red-brown powder. Yield: 0.17 g (83.8 %). Anal. Calcd for $C_{45}H_{37}N_9ORu$ (%): C, 65.84; H, 4.54; N, 15.36. Found (%): C, 65.83; H, 4.58; N, 15.35. ^{1}H NMR (400 MHz, DMSO-d_6): δ (ppm) 10.06 (d, $J = 8.2$ Hz, 2H), 8.89 (m, 6H), 8.27 (m, 4H), 8.10 (t, $J = 6.8$ Hz, 4H), 7.83 (m, 3H), 7.61 (t, $J = 7.6$ Hz, 2H), 7.37 (t, $J = 7.8$ Hz, 2H), 3.02 (t, $J = 7.6$ Hz, 4H), 2.27 (t, $J = 7.8$ Hz, 2H), 1.75 (t, $J = 7.4$ Hz, 2H), 1.27 (m, 4H). ES-MS (CH_3CN): *m/z* 821 ([M − 2ClO$_4$ + H]$^+$), 411 ([M − 2ClO$_4$]$^{2+}$). CD (H_2O): λ/nm ($\Delta\varepsilon$/M^{-1} cm^{-1}) 472 (−13.3), 420 (15.9), 292 (−196.8), 276 (73.3), 239 (17.6).

Λ-Ru3

Λ-[Ru(bpy)$_2$(HQIP)](ClO$_4$)$_2$ (**Λ-Ru3**) was synthesized in a manner identical to that described for Δ-[Ru(bpy)$_2$(HQIP)](ClO$_4$)$_2$, but using Λ-[Ru(bpy)$_2$(py)$_2$][*O*,*O*′-dibenzoyl-L-tartrate]·12H$_2$O (0.20 g, 0.2 mmol) rather than Δ-[Ru(bpy)$_2$(py)$_2$][*O*,*O*′-dibenzoyl-D-tartrate]·12H$_2$O. Yield: 0.18 g (87.8 %). The elemental analysis, ^{1}H NMR, and mass spectral data for **Λ-Ru3** were the same as those for **Δ-Ru3**, within experimental error. CD (H_2O): λ/nm ($\Delta\varepsilon$/M^{-1} cm^{-1} 472 (12.9), 420 (−14.7), 292 (190.0), 276 (−70.5), 239 (−16.9).

Physical measurements

Microanalysis (C, H, and N) was performed using a Vario EL elemental analyzer. ^{1}H NMR spectra were recorded at room temperature with a Bruker AVANCE AV 400-NMR spectrometer using DMSO-d_6 as the solvent and tetramethylsilane as the internal standard. Fast atom bombardment mass spectra were acquired using a VG ZAB-HS spectrometer in a 3-nitrobenzyl alcohol matrix. Electrospray mass spectra were recorded with an LCQ system (Finnigan MAT, USA). The spray voltage, tube lens offset voltage, capillary voltage, and capillary temperature were set to 4.50 kV, 30.00 V, 23.00 V, and 200 °C, respectively, and the quoted *m/z* values are for the major peaks in the isotope distribution. The CD spectra were measured with a JASCO J810 spectrometer.

Cell lines and cell culture

Human cancer cell lines, including the HepG2 hepatocellular carcinoma cell line, the HeLa cervical carcinoma cell line, and the MCF-7 breast carcinoma cell line, were purchased from American Type Culture Collection (Manassas, VA, USA). The A549 human lung carcinoma cell line, the cisplatin-resistant cell line A549-CP/R, the MG63 osteosarcoma cell line, the BEL-7402 hepatocellular carcinoma cell line, and LO2 normal hepatic cells were obtained from the cell bank of the Cell Institute of Sinica Academia Shanghai (Shanghai, China). All cell lines were cultured in 25-cm^2 culture flasks in either RPMI-1640 medium (Invitrogen, Carlsbad, CA, USA) or Dulbecco's modified Eagle's medium (Gibco, Gaithersburg, MD, USA) supplemented with fetal bovine serum (10 %), penicillin

(100 U/mL), and streptomycin (50 U/mL) at 37 °C in a CO_2 incubator (95 % relative humidity, 5 % CO_2). The cells were cultured until they reached the logarithmic growth phase unless otherwise specified.

Cytotoxicity assay

The standard MTT assay was used to assess the cytotoxicity as previously described [39]. Cells were adjusted to the proper concentration, seeded in 96-well microplates, and incubated overnight at 37 °C in a 5 % CO_2 incubator. After serial dilutions of the ruthenium(II) complexes had been added, the cells were incubated for an additional 48 h. The negative control cells were treated with the vehicle, and cisplatin was used as a positive control agent. Wells containing culture medium without cells were used as blanks. On completion of the incubation, MTT solution [MTT working solution, 5 mg/mL phosphate-buffered saline (PBS), 20 μL per well] was added, and the cells were incubated for 4 h. Then, the medium was aspirated and replaced with 150 μL of 2-propanol per well to dissolve the formazan. The optical density of each well was measured using a microplate reader at a wavelength of 570 nm. The half-maximal inhibitory concentration (IC_{50}) was determined by a plot of the viability versus the dose used to treat the cells. All data were from at least three independent experiments and are expressed as the mean ± the standard deviation.

Inductively coupled plasma mass spectrometry

ICP-MS (Thermo Elemental system) was used to quantify the levels of ruthenium in different subcellular compartments, as described in our previous report [40]. HeLa cells were cultured in 25-cm^2 culture plates (Corning) and incubated with the six ruthenium(II) complexes at the same concentration of 20 μM for 48 h. The cytoplasmic, nuclear, and mitochondrial fractions were obtained. Aliquots were removed and used to determine the protein concentration using bicinchoninic acid (Pierce, Rockford, IL, USA). The results are reported as nanograms of ruthenium per milligram of cellular protein. The data are reported as the mean ± the standard deviation ($n = 3$).

Cellular localization analysis

HeLa cells were adjusted to the proper concentration and seeded on 35-mm glass-bottomed culture dishes. When the cells reached more than 60 % confluency, the ruthenium(II) complexes were added at a concentration of 10 μM, and the cells were incubated for 48 h. Then, DAPI (5 μg/mL) was added to the dishes, which were incubated for 5 min. The cells were washed with 1 mL of PBS before the samples were observed under an inverted fluorescence microscope (Zeiss Axio Observer D1) [41].

To evaluate the intracellular localization of the ruthenium(II) complexes, we examined the extent of color merging using the endoplasmic-reticulum-specific probe ER-Tracker Green and the mitochondria-specific probe Mito-Tracker Green FM [42, 43]. HeLa cells were treated as described earlier, and then, Mito-Tracker Green FM or ER-Tracker Green was added to the dishes. After incubation for 15 min, the dishes were washed with 1 mL of PBS and the samples were observed under an inverted fluorescence microscope (Zeiss Axio Observer D1).

Annexin V staining to detect early-phase apoptosis

Early-phase apoptosis was detected by annexin V staining. HeLa cells were adjusted to the proper concentration, seeded in six-well culture plates, and incubated overnight at 37 °C in a 5 % CO_2 incubator. Then, the ruthenium(II) complex (15 μM) was added, and the cells were incubated for 0–36 h. The cells were trypsinized, washed twice with cold PBS, and then resuspended in 100 μL of binding buffer [50 mmol/L *N*-(2-hydroxyethyl)piperazine-*N*′-ethanesulfonic acid/NaOH, pH 7.4, 700 mmol/L NaCl, 12.5 mmol/L $CaCl_2$] containing 5 μL of annexin V stock solution (Invitrogen, Paisley, UK). After the cells had been incubated for 15 min at room temperature in a light-protected area, 400 μL of binding buffer was added, and the specimens were quantified by flow cytometry (FACSCanto II, BD Biosciences, San Jose, CA, USA).

DAPI staining to detect late-phase apoptosis

HeLa cells were prepared as described earlier. At different time points, cells were stained with DAPI to analyze nuclear fragmentation. The cells were fixed with 4 % formaldehyde in PBS for 15 min, washed twice with PBS, and then permeabilized with 0.2 % Triton X-100 in PBS for 5 min. Next, the cells were washed with cold PBS before incubation with DAPI (5 μg/mL) for 10 min at room temperature, and then the DAPI-stained cells were washed twice with PBS. The samples were observed under an inverted fluorescence microscope [44].

Measurement of intracellular reactive oxygen species

Accumulation of reactive oxygen species (ROS) was quantified using the DCFH-DA assay. DCFH-DA is a nonfluorescent compound that becomes the highly fluorescent 2′,7′-dichlorofluorescein on oxidation by intracellular ROS. HeLa cells were treated with ruthenium(II) complexes or H_2O_2 at different concentrations for 6 h, and untreated cells were used as a control. Then, the cells were

incubated with 10 μM DCFH-DA (Sigma-Aldrich) for 30 min at 37 °C. The intracellular fluorescence intensity of the cells was measured using a flow cytometer (FACSCanto II, BD Biosciences, San Jose, CA, USA) and a microplate analyzer (Infinite M200, Tecan, Männedorf, Switzerland). When necessary, *N*-acetylcysteine (NAC; 10 mM) was applied 1 h before the treatment with the ruthenium(II) complexes or H_2O_2 and was kept in the medium during treatment until the cells were analyzed. The excitation wavelength was 488 nm, and the fluorescence was measured at 530 nm. The acquisition and analysis of the flow cytometry data were performed using FlowJo.

Evaluation of the mitochondrial membrane potential

Mitochondrial dysfunction was detected by measuring changes in the mitochondrial membrane potential using an inverted fluorescence microscope and flow cytometry after live cells had been stained with 5,5′,6,6′-tetrachloro-1,1′,3,3′-tetraethylbenzimidazolylcarbocyanine iodide (JC-1) [45]. For microscopic observation, HeLa cells were adjusted to the proper concentration and seeded in six-well plates. When the cells reached more than 60 % confluency, the ruthenium(II) complexes were added at a concentration of 15 μM, and the cells were incubated for 0–12 h. Then, the cells were incubated for 30 min in complete medium containing 5 mg/mL JC-1. After they had been washed twice with PBS, the stained cells were analyzed using an inverted fluorescence microscope.

For flow cytometry analysis, HeLa cells were prepared as described earlier and incubated with the ruthenium(II) complexes at concentrations of 5, 10, and 20 μM for 6 h. After exposure to the complexes, the cells were trypsinized and resuspended in 0.5 mL of PBS containing 5 mg/mL JC-1. After the cells had been incubated for 30 min in the dark, the supernatant was immediately removed by centrifugation. Next, the cells were washed and resuspended in PBS, and the stained cells were immediately analyzed by flow cytometry. The relative intensities of the green fluorescence signals from JC-1 monomers were used to show the cells that lost mitochondrial membrane potential.

Transmission electron microscopy

HeLa cells (5×10^5) were treated with the ruthenium(II) complexes (15 μM) for 24 h. The cells were washed twice and fixed with 2 % glutaraldehyde at 4 °C for 1 h and postfixed with 2 % osmium tetroxide. The cells were then dehydrated with sequential washes in ethanol and embedded in Spurr resin. The ultrathin sections obtained were mounted on copper grids, counterstained with uranyl acetate and lead citrate, and then visualized using an electron microscope (JEM 100 CX, JEOL, Tokyo, Japan). Images were taken and scanned using the program Eversmart Jazz (Scitex).

Western blot analysis

Exponentially growing HeLa cells were treated with the ruthenium(II) complexes (15 μM) for 6–48 h (1–24 h for detection of cytochrome *c*). For the preparation of whole-cell or cytoplasmic protein extracts [46], at each time point, cells were washed twice with ice-cold PBS and lysed in radioimmunoprecipitation assay buffer {50 mM tris(hydroxymethyl)aminomethane–HCl, 150 mM NaCl, 0.1 % sodium dodecyl sulfate, 1 % NP-40, 0.5 % sodium deoxycholate, 1 mM phenylmethanesulfonyl fluoride, 100 mM leupeptin, and 2 mg/mL aprotinin, pH 8.0] to extract the total cellular proteins. The protein extracts were resolved using 10 % sodium dodecyl sulfate–polyacrylamide gels loaded with equal amounts of the proteins per lane. Equal amounts of protein (20–50 μg) were electrophoresed on 10 % or 15 % sodium dodecyl sulfate–polyacrylamide gels. Next, the proteins were electroblotted onto Immobilon-P poly(vinylidene difluoride) transfer membranes (Millipore, Bedford, MA, USA), which were then blocked with 5 % nonfat milk in a buffer consisting of 50 mM tris(hydroxymethyl)aminomethane, pH 7.6, 150 mM NaCl, and 0.1 % Tween 20 on a shaker at room temperature for 1 h. Then, the membranes were probed with primary antibodies (Epitomics, Burlingame, CA, USA) at 1:1,000 dilution in 5 % nonfat milk overnight at 4 °C and then with secondary antibodies (goat anti-rat, Santa Cruz Biotechnology, Santa Cruz, CA, USA) conjugated with horseradish peroxidase at 1:2,000 dilution for 1 h at room temperature. To ensure the presence of comparable amounts of proteins in each lane, the membranes were stripped and probed for glyceraldehyde 3-phosphate dehydrogenase (Santa Cruz Biotechnology, Santa Cruz, CA, USA). The protein bands were visualized using electrochemiluminescence detection reagents according to the instructions for the SuperSignal West Pico kit (Pierce Biotechnology, Rockford, IL, USA).

Results and discussion

Synthesis and characterization

The synthesis of the ruthenium(II) complexes (**Δ-Ru1**, **Λ-Ru1**, **Δ-Ru2**, **Λ-Ru2**, **Δ-Ru3**, and **Λ-Ru3**) is illustrated in Scheme S1. These complexes were characterized by ^{1}H NMR spectroscopy, ES-MS, CD spectroscopy, and elemental analysis. $[M - 2ClO_4 - H]^+$ and $[M - 2ClO_4]^{2+}$ signals were observed in the ES-MS spectra of the ruthenium(II) complexes. The enantiomers yielded identical,

well-defined ^{1}H NMR spectra, which permitted unambiguous identification and the assessment of purity. The enantiomeric purity of these complexes was assayed by CD spectroscopy. **Δ-Ru1**, **Δ-Ru2**, and **Δ-Ru3** exhibited two primary CD signals, with a positive peak at approximately 275 nm and a negative peak at approximately 291 nm. As expected, the opposite patterns were observed for the enantiomers **Λ-Ru1**, **Λ-Ru2**, and **Λ-Ru3** (Fig. S1).

Cytotoxicity study

We examined the in vitro cytotoxic activity of these ruthenium(II) complexes against six selected human cancer cell lines (HeLa, A549, HepG2, MCF-7, BEL-7402, and MG-63), one cisplatin-resistant cell line (A549-CP/R), and a normal human liver cell line (LO2) using the MTT assay. Cisplatin was used as a positive control. As shown in Table 1, **Δ-Ru1** exhibited cytotoxicity similar to that of cisplatin against the six cancer cell lines. Notably, this complex could inhibit the growth of the cisplatin-resistant cell line A549-CP/R, suggesting that the anticancer mechanism of **Δ-Ru1** differs from that of cisplatin and that this complex could help overcome the challenges associated with the emergence of cisplatin resistance in cancer therapy. In addition, **Δ-Ru1** was found to have potent toxicity against tumor cells and was much less toxic than cisplatin to the normal human liver cell line (LO2), indicating that **Δ-Ru1** most likely has a better therapeutic profile than cisplatin. Because HeLa cells exhibited the highest sensitivity to **Δ-Ru1**, we used this cell line as the cell model for further investigation.

Cellular uptake and subcellular distribution

The six ruthenium(II) complexes, with similar ligands, displayed very different cytotoxicity in vitro. Our previous study had showed the cellular uptake of the ruthenium(II) complex was important for the cytotoxicity in vitro [22, 40]. So we used live-cell imaging and ICP-MS to determine the distribution of the ruthenium(II) complexes in the HeLa cells to address this question. Live-cell imaging showed that most of these complexes were distributed in the cytoplasm when cells were incubated with these complexes at a concentration half the IC_{50} value for 48 h (Fig. S2). Furthermore, ICP-MS showed that after exposed to the same concentration of these six ruthenium (II) complexes in the same time, the quantitative order of ruthenium in the whole-cell lysates was as follows: **Δ-Ru1** ≈ **Λ-Ru1** > **Δ-Ru2** ≈ **Λ-Ru2** > **Δ-Ru3** ≈ **Λ-Ru3** (Fig. 2). These data suggested that there was a positive relationship between the cellular uptake and the in vitro cytotoxicity for the HeLa cells. The highest level of ruthenium in the whole-cell lysates (125 ± 11 ng of ruthenium per milligram of protein) was found for **Δ-Ru1**, and this complex was the most active anticancer agent (IC_{50} = 9.3 ± 2.1 μM for HeLa). **Λ-Ru1** displayed slightly lower toxicity than **Δ-Ru1**, which also seems to be attributed to the slightly less cellular uptake of ruthenium; in HeLa cells, the same relationship was found for **Δ-Ru2** and **Λ-Ru2**, but the opposite relationship was found for **Δ-Ru3** and **Λ-Ru3**.

Most of **Δ-Ru1** and **Λ-Ru1** accumulated in the mitochondrial fraction of HeLa cells and they could hardly be detected in the nucleus. In contrast, **Δ-Ru2**, **Λ-Ru2**, **Δ-Ru3**, and **Λ-Ru3** were found in the mitochondria, nucleus, and cytoplasm. This significant difference in subcellular distribution is probably another factor that is responsible for the disparity in cytotoxicity among these ruthenium(II) complexes.

Cellular localization analysis

We used fluorescence microscopy to obtain further information on the exact cellular localization of **Δ-Ru1** and **Λ-Ru1**,

Table 1 Half-maximal inhibitory concentrations (IC_{50}) of the ruthenium(II) complexes and cisplatin toward different tumor cell lines

Cell line	IC_{50} (μM)						
	Δ-Ru1	**Λ-Ru1**	**Δ-Ru2**	**Λ-Ru2**	**Δ-Ru3**	**Λ-Ru3**	Cisplatin
HeLa (ovary)	9.3 ± 2.1	17.1 ± 3.5	20.7 ± 5.6	34.6 ± 3.5	69.5 ± 7.8	61.9 ± 5.6	10.5 ± 1.8
HepG2 (liver)	13.6 ± 2.2	21.3 ± 4.5	151.8 ± 10.3	179.2 ± 12.5	76.5 ± 8.9	57.9 ± 5.3	14.6 ± 2.4
BEL-7402 (liver)	17.6 ± 3.2	22.9 ± 3.6	153.7 ± 12.6	161.3 ± 13.5	156.2 ± 14.5	130.8 ± 9.1	19.7 ± 3.2
MG-63 (osteosarcoma)	12.7 ± 1.4	18.7 ± 3.5	47.9 ± 5.6	36.0 ± 3.8	126.1 ± 12.8	105.9 ± 9.6	7.5 ± 1.6
MCF-7 (breast)	10.6 ± 1.3	22.1 ± 7.8	242.2 ± 21.3	227.6 ± 21.4	255.6 ± 22.4	251.7 ± 26.2	9.5 ± 1.2
A549 (lung)	16.2 ± 3.2	34.8 ± 6.3	182.4 ± 14.7	170.6 ± 18.7	112.2 ± 14.5	87.1 ± 4.2	18.2 ± 3.5
A549-CP/R (lung)	26.9 ± 4.5	30.3 ± 5.6	246.2 ± 12.5	220.4 ± 11.3	156.5 ± 12.4	86.5 ± 5.8	60.5 ± 5.7
LO2 (liver)	88.9 ± 5.6	90.3 ± 5.6	212 ± 12.5	190.4 ± 11.3	162 ± 13.4	76.5 ± 8.8	14.5 ± 5.7

See Fig. 1 for the structures of the ruthenium(II) complexes. The data are presented as the mean ± the standard deviation, and cell viability was assessed after 48 h of incubation. A549-CP/R is a cisplatin-resistant cell line and LO2 is a human normal liver cell line

Δ-Ru2 and **Λ-Ru2**, and **Δ-Ru3** and **Λ-Ru3**. Live-cell imaging showed that **Δ-Ru1** and **Λ-Ru1** were limited to the cytoplasm and were not present in the nucleus of HeLa cells stained with DAPI (Figs. 3a–d, 4a–d). In previous studies, it was found that ruthenium(II) complexes can induce cancer cell apoptosis by activating the intrinsic mitochondrial pathways or endoplasmic reticulum pathways [47, 48]. Therefore, in this study, colocalization experiments were used to determine if **Δ-Ru1** and **Λ-Ru1** were localized to the mitochondria or endoplasmic reticulum. As shown in Figs. 3h and 4h, excellent superimposition, indicated by the yellow color, between the signals for **Δ-Ru1** or **Λ-Ru1** (red) and MitoTracker Green FM (green) was observed; however, there was no overlap between ER-Tracker Green (green) and **Δ-Ru1** or **Λ-Ru1** (Figs. 3l, 4l). Results were also obtained for **Δ-Ru2** and **Λ-Ru2** and for **Δ-Ru3** and **Λ-Ru3** (Figs. S3–S6). Among these six ruthenium(II) complexes, the best colocalization with the mitochondria was for **Δ-Ru1**. Taken together, the ICP-MS and live-cell imaging results indicated that **Δ-Ru1** primarily accumulated in the mitochondria, and thus mitochondria may be its primary target. On the basis of its having the best anticancer effect among these six complexes and its targeting of mitochondria, the rest of the study focused on the biological properties of **Δ-Ru1** for further investigation.

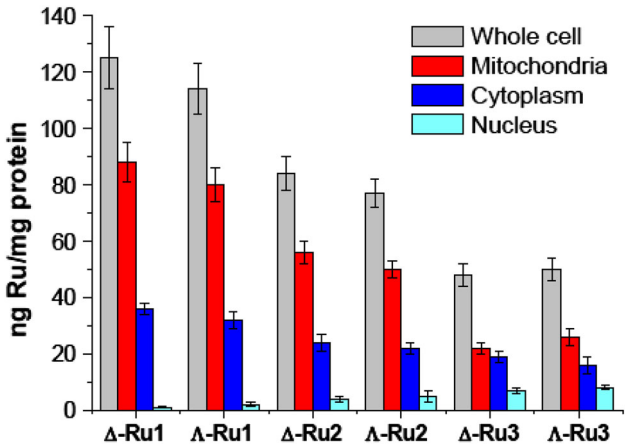

Fig. 2 Subcellular accumulation of ruthenium(II) complexes determined in HeLa cells after 48 h of exposure to the same concentration of 20 μM

Apoptosis assays

To determine whether **Δ-Ru1** causes cell death by apoptosis or necrosis, annexin V and DAPI staining assays were performed. The externalization of phosphatidylserine on the outer surface of the plasma membrane is a known hallmark of early-phase apoptosis, and therefore the binding of annexin V to the cell surface is an indication of early-phase apoptosis [49, 50]. Flow cytometry revealed

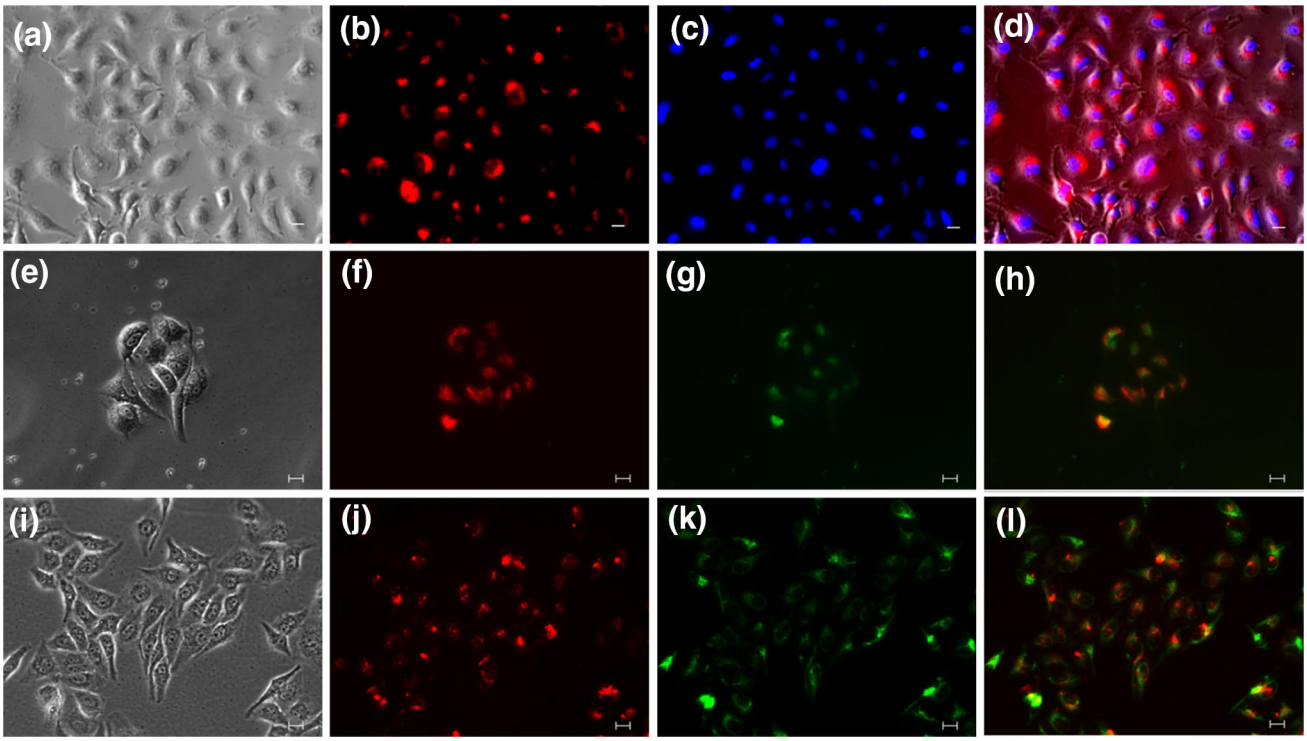

Fig. 3 Cell localization imaging of **Δ-Ru1** (10 μM). **a**, **e**, **i** Bright field images. **b**, **f**, **j** Luminescence images of **Δ-Ru1** (*red*). **c** Luminescence image of 4′,6-diamino-2-phenylindole (DAPI; *blue*). **g** Luminescence image of MitoTracker Green FM (*green*). **k** Luminescence image of ER-Tracker Green (*green*). **d**, **h**, **l** Merged pictures. *Scale bar* 20 μm

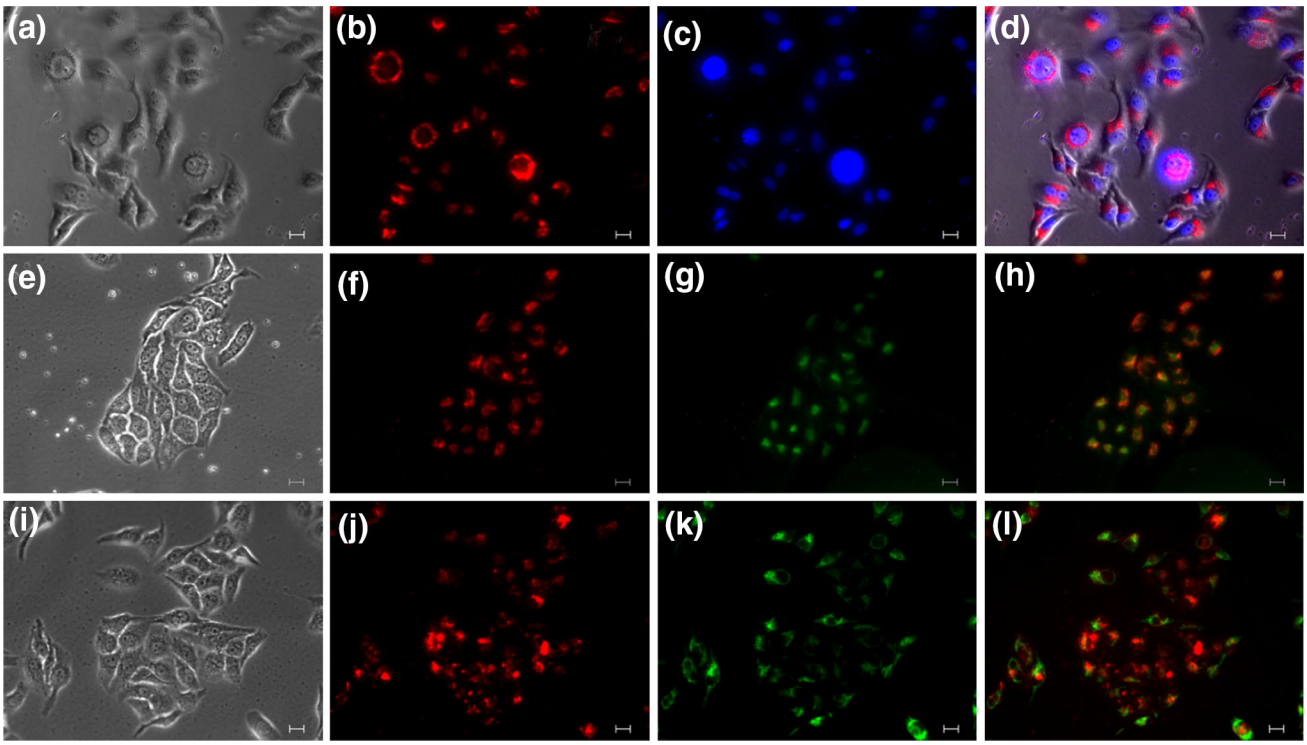

Fig. 4 Cell localization imaging of **Λ-Ru1** (10 μM). **a**, **e**, **i** Bright field images. **b**, **f**, **j** Luminescence images of **Λ-Ru1** (*red*). **c** Luminescence image of DAPI (*blue*). **g** Luminescence image of MitoTracker Green FM (*green*). **k** Luminescence image of ER-Tracker Green (*green*). **d**, **h**, **l** Merged pictures. *Scale bar* 20 μm

that early-phase apoptosis was induced in HeLa cells by 3 h of treatment with **Δ-Ru1** (15 μM), and as the exposure time increased, the percentage of annexin V-positive cells increased (Fig. 5). Nuclear condensation and fragmentation are considered indicative of late-phase apoptosis [51, 52]. These characteristics can be detected by DAPI, which is a DNA-binding dye that has been used extensively for staining cell nuclei [53]. For this purpose, HeLa cells were treated with **Δ-Ru1** (15 μM) for various time periods, and then the cell nuclei were stained with DAPI. As expected, the cell nuclei shrank after exposure for 6 h, and these effects were severer with increasing exposure time. Nuclear condensation and fragmentation were obvious after 48 h (Fig. 6). On the basis of the results of the two apoptosis assays, we concluded that the cytotoxic effects of **Δ-Ru1** on HeLa cells are primarily caused by apoptosis.

Intracellular ROS study

ROS include the superoxide radical ($O_2^{\cdot -}$), hydrogen peroxide (H_2O_2), and the hydroxyl radical (OH·). Oxidative stress generated by an imbalance between ROS and antioxidants contributes to the pathogenesis of cancer, respiratory diseases, and some toxic diseases [54]. NAC is a source of sulfhydryl groups in cells and is a scavenger of free radicals as it interacts with ROS such as OH· and H_2O_2 [55]. It has been reported that ROS have an important role in the induction of apoptosis by some ruthenium(II) complexes [27, 40, 56]. However, another study showed that ROS were not produced during treatment with ruthenium(II) complexes [28]. We therefore investigated whether **Δ-Ru1** could increase the ROS level in HeLa cells. Flow cytometry showed a slight concentration-dependent increase in the amount of ROS compared with the amount in the vehicle-treated cells (Fig. 7a). To further examine the role of ROS generation in ruthenium(II)-induced cytotoxicity, we used H_2O_2 as a positive control and NAC as the ROS scavenger. The results showed that pretreatment of the cells with NAC could abrogate both H_2O_2-induced and ruthenium(II)-induced ROS generation (Fig. 7b). Furthermore, the presence of NAC significantly suppressed H_2O_2-induced cytotoxicity, but interestingly, the presence of NAC could not reduce the cytotoxicity of **Δ-Ru1** toward HeLa cells (Fig. 7c). Taken together, these results indicate that **Δ-Ru1** can induce the production of a small amount of ROS, but ROS production is not the crucial factor in the apoptosis of HeLa cells induced by **Δ-Ru1**.

Induction of mitochondrial dysfunction

Mitochondria play a crucial role in apoptosis triggered by chemical agents. Chemical-induced apoptosis mediated by

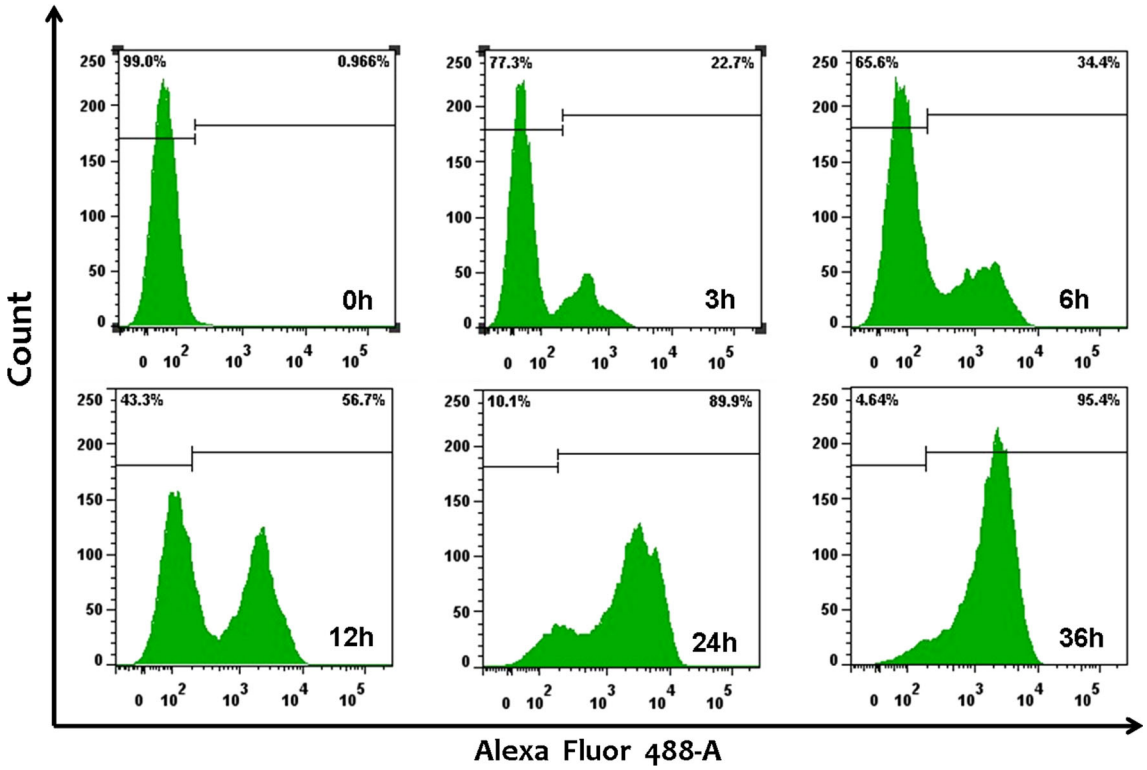

Fig. 5 Early-phase apoptosis of HeLa cells induced by **Δ-Ru1** was examined by the annexin V assay. HeLa cells were treated with **Δ-Ru1** (15 μM) for 0–36 h and then analyzed by flow cytometry

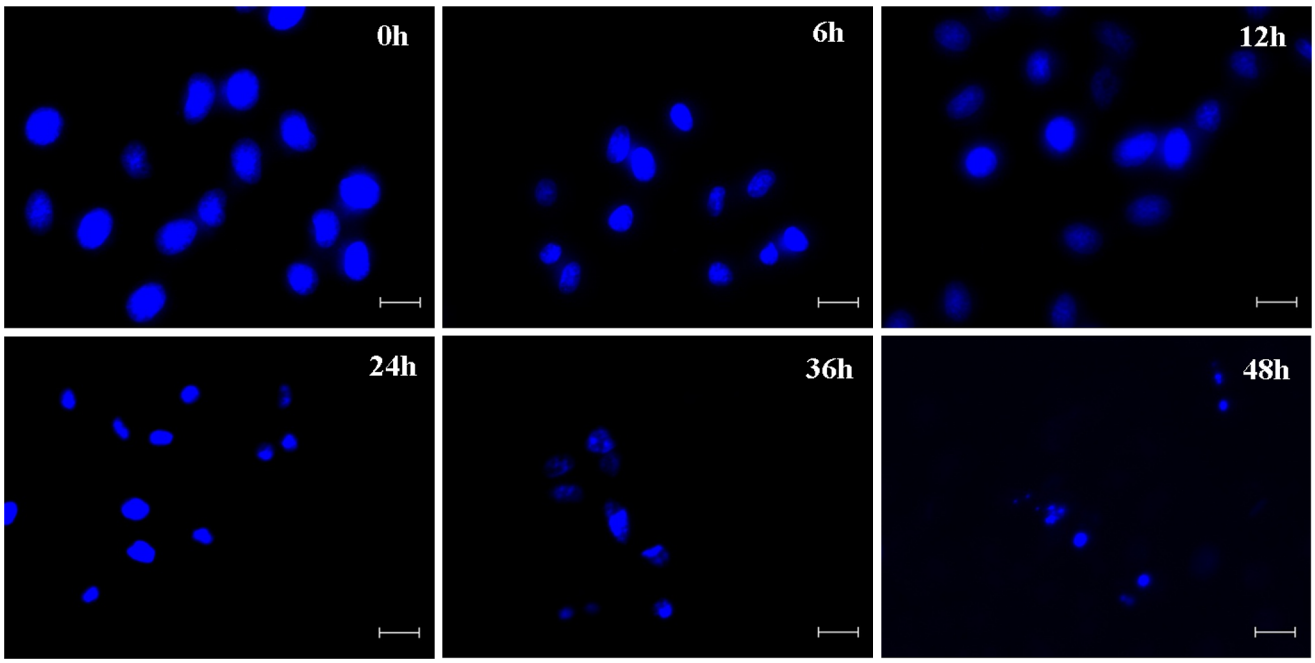

Fig. 6 Late-phase apoptosis of HeLa cells induced by **Δ-Ru1** was examined by analyzing nuclear fragmentation with DAPI staining. HeLa cells were treated with **Δ-Ru1** (15 μM) for 0–48 h. *Scale bar* 20 μm

the mitochondria/apoptotic cascades is often associated with the collapse of the mitochondrial membrane potential as a result of the leakage of proapoptotic factors [57]. Very recently, it has been reported that ruthenium(II) complexes can induce cell death by interfering with the membrane potential, finally leading to apoptosis [27, 28, 34, 35]. To

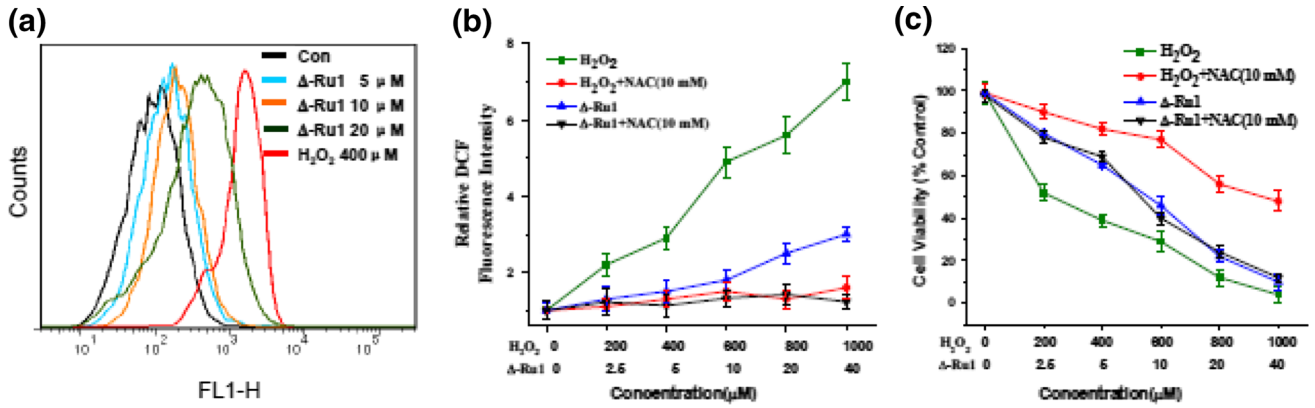

Fig. 7 **a** Analysis of production of reactive oxygen species (ROS) after HeLa cells had been treated with **Δ-Ru1** for 6 h. The intracellular ROS level was detected by flow cytometry (FL-1 channel; excitation at 488 nm and emission at 525 nm). **b** The ROS level was expressed as the relative fluorescence intensity measured with a microplate reader after 6 h of treatment with the ruthenium(II) complex and H_2O_2 with or without antioxidants (*N*-acetylcysteine, *NAC*) at the concentrations indicated. The data are presented as mean ± the standard deviation and were obtained in three independent experiments. **c** Effects of NAC (10 mM) on **Δ-Ru1**-induced or H_2O_2-induced cytotoxicity. HeLa cells were exposed to different doses of **Δ-Ru1** or H_2O_2 with or without NAC for 48 h. Cell viability was assessed by the 3-(4,5-dimethylthiazol-2-yl)-2,5-diphenyltetrazolium bromide assay. *Con* control, *DCF* 2′,7′-dichlorofluorescein

investigate the role of this mechanism, the lipophilic cationic molecular probe JC-1 was used to determine whether **Δ-Ru1** can induce alterations in the mitochondrial membrane potential. JC-1 exhibits potential-dependent accumulation in the mitochondria, and the loss of mitochondrial membrane potential can be visualized by a fluorescence shift from red (590 nm) to green (525 nm) [58]. After cells had been treated with **Δ-Ru1** for 6 h, there was a significant dose-dependent decrease in the ratio of red to green fluorescence in HeLa cells (Fig. 8a). In addition, when HeLa cells were incubated with **Δ-Ru1** at a concentration of 15 μM, a rapid depolarization of the mitochondrial membrane potential was detected starting at 0.5 h, reaching a maximum at 12 h (Fig. 8b). These results are in accordance with the time course of apoptosis observed in HeLa cells (as showed in Figs. 5, 6) and suggest that the collapse of the mitochondrial membrane potential is an early event in **Δ-Ru1**-induced apoptosis. As mentioned earlier, cancer cells have higher mitochondrial membrane potential than their normal counterparts and are more sensitive to damage by mitochondria-targeting agents [25, 26], which may partly account for the toxicity of **Δ-Ru1** toward tumor cells over nonmalignant cells.

To analyze further the mitochondrial morphological alterations caused by treatment with the ruthenium complex, transmission electron microscopy studies were performed using HeLa cells that had been treated with **Δ-Ru1** (15 μM) for 24 h. The control cells were characterized by a normal morphology for the cytoplasm, nucleus, and mitochondria (Fig. 8c, images a and b). In contrast, the treated cells had an apoptotic morphology and abnormally swollen mitochondria (Fig. 8c, images c and d), indicative of the loss of mitochondrial membrane potential [56].

Apoptosis induced through the intrinsic mitochondrial pathway

There are two primary signaling pathways involved in apoptosis: the extrinsic (receptor-mediated) and intrinsic (mitochondria-mediated) pathways [59]. The crucial step in the intrinsic pathway is the loss of mitochondrial membrane potential and release of cytochrome *c*, which occur as early initiating events before caspase-mediated activation of apoptotic cascades [60]. The mitochondrial response to the disruption of the mitochondrial membrane potential includes the release of cytochrome *c* into the cytosol. In the cytosol, cytochrome *c* binds to Apaf-1, allowing the recruitment of caspase-9 and the formation of an apoptosome complex, resulting in caspase-3 activation and the execution of cell death [61–63]. To assess whether **Δ-Ru1** initiates apoptosis through this signaling pathway, we determined whether this complex can trigger the release of cytochrome *c* from the mitochondria. Western blot analysis showed that the cytochrome *c* level in the whole cell did not obviously change, whereas the release of cytochrome *c* was detected at 1 h in the cytosol after treatment. This ruthenium(II) complex induced an obvious time-dependent increase in the cytochrome *c* level in the cytosol (Fig. 9a). These results clearly showed that the induction of apoptosis by **Δ-Ru1** began with the collapse of the mitochondrial membrane potential, which resulted in the permeabilization of the mitochondrial outer membrane. This permeabilization in turn led to the release of cytochrome *c* from the mitochondria, inducing apoptosis.

Apoptosis is executed by the concerted activation of caspases, including initiator (caspase-9) and executioner (caspase-3) caspases. To determine further the involvement

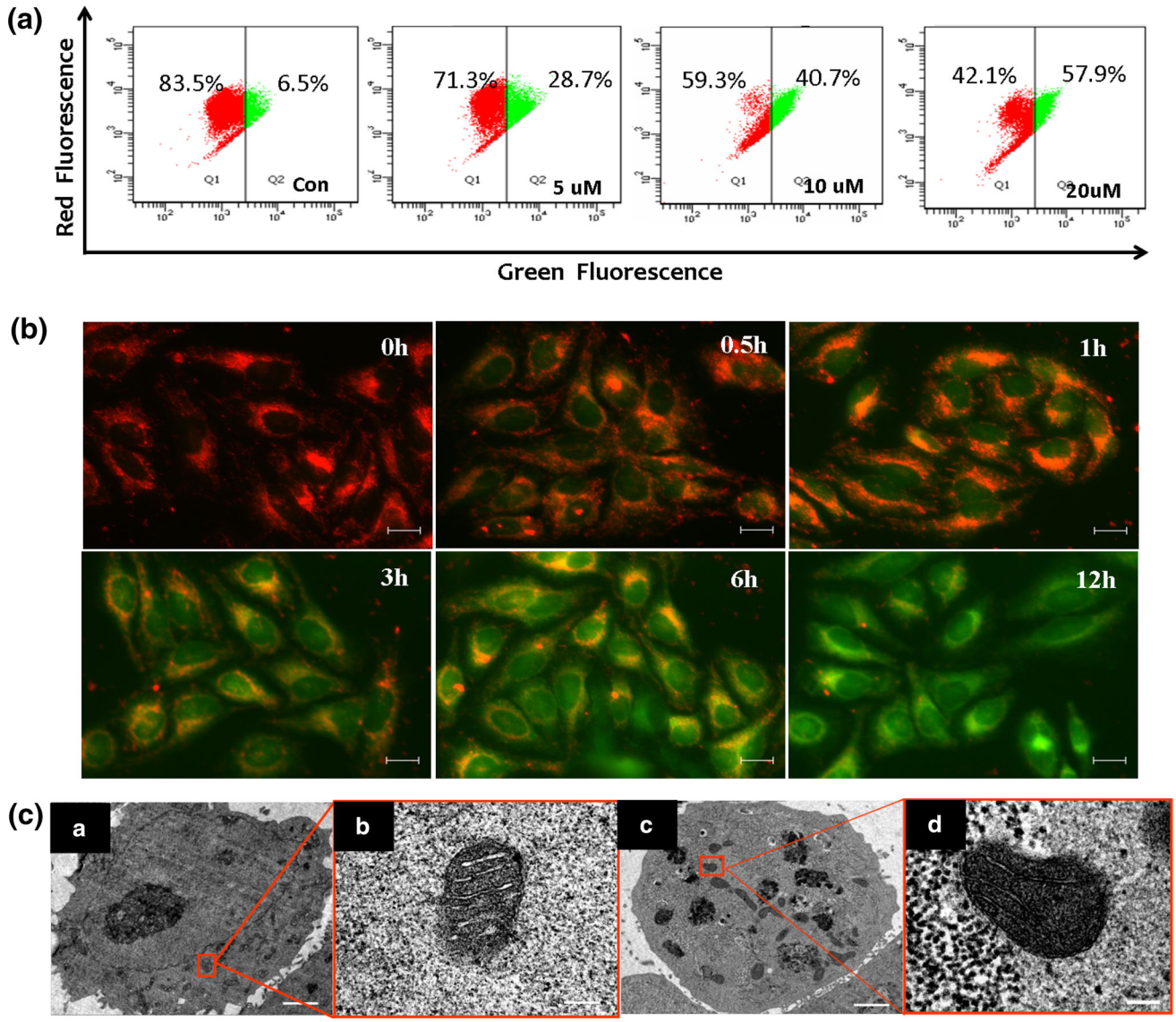

Fig. 8 **a** Depletion of mitochondrial membrane potential in HeLa cells after treatment with **Δ-Ru1** for 6 h and analyzed by flow cytometry. The data are the mean of three independent experiments. **b** Fluorescence images of 5,5′,6,6′-tetrachloro-1,1′,3,3′-tetraethylbenzimidazolylcarbocyanine iodide-labeled HeLa cells treated with **Δ-Ru1** (15 μM) for 0–12 h taken with an inverted fluorescence microscope. *Scale bar* 20 μm. **c** Impact of **Δ-Ru1** on mitochondrial morphology observed by transmission electron microscopy: control (*a*); magnified normal mitochondria (*b*); HeLa cells treated with **Δ-Ru1** (15 μM) for 24 h (*c*); magnified abnormal (swollen) mitochondria (*d*). *Scale bar* 1 μm for *a* and *c*, and 0.1 μm for *b* and *d*

of caspase-9 and caspase-3 in **Δ-Ru1**-induced apoptosis, we determined the levels of the uncleaved and cleaved (active) forms of caspase-9 and caspase-3 in cell lysates. As shown in Fig. 9b, the level of uncleaved caspase-9 (47 kDa) was reduced in parallel with a time-dependent increase in the level of its active subunit (35 kDa) after 6 h of treatment with **Δ-Ru1**. Subsequently, the active cleaved form of caspase-3 (17 kDa) was detected after caspase-9 activation at 24 h, consistent with the fact that caspase-3 is activated by caspase-9 during apoptosis. As an irreversible hallmark of apoptosis [64], the cleavage of caspase-3 (17 kDa) indicates that HeLa cells treated with **Δ-Ru1** completed the apoptosis process. All of these results together indicate that **Δ-Ru1**-induced apoptotic death is mediated by mitochondria-dependent signaling pathways. Prosurvival factors such as Bcl-2 and Bcl-xl can maintain the integrity of the mitochondrial outer membrane, whereas proapoptotic factors, such as Bax, can disrupt its integrity, causing the release of proapoptotic factors into the cytosol. Increasing the Bax to Bcl-2 or Bax to Bcl-xl ratio could induce the permeabilization of mitochondria [65, 66]. Many studies have reported that Bcl-2 family members are important key regulators of mitochondrial function during apoptosis induced by ruthenium(II) complexes [27, 34–36, 40]. Although most studies

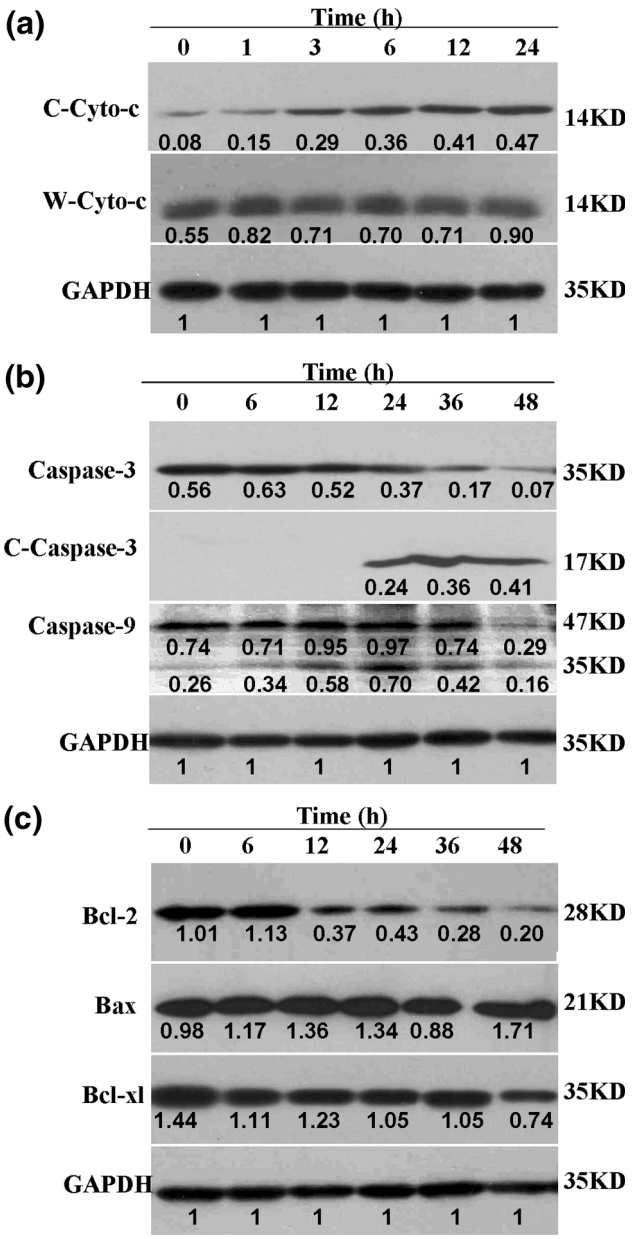

Fig. 9 Effect of **Δ-Ru1** on the apoptotic pathway in HeLa cells. **a** Release of cytochrome *c*. HeLa cells were treated with **Δ-Ru1** (15 μM) for 0–24 h. Cells were homogenized, and lysates (cytosolic fraction and the whole cells) were assayed for cytochrome *c* levels (*C-Ctoc-c* is the cytochrome *c* level in the cytosol, and *W-Ctoc-c* is the cytochrome *c* level in the whole cell) using Western blot analysis. **b**, **c** Effect of **Δ-Ru1** on the expression of apoptosis-related proteins. HeLa cells were treated with **Δ-Ru1** (15 μM) for 0–48 h. Whole-cell lysate was prepared and subjected to Western blotting for cytochrome *c*, caspase-3, cleaved caspase-3 (*C-caspase-3*), caspase-9, Bax, Bcl-2, and Bcl-xl. *GAPDH* glyceraldehyde 3-phosphate dehydrogenase

have concentrated on the dose–response relationship, in this study, we assessed the time dependence of the effects on Bcl-2 family members to elucidate the detailed process by which the ruthenium(II) complex induces apoptosis. We found that **Δ-Ru1** treatment greatly downregulated the expression level of the prosurvival protein Bcl-xl after 6 h, and the Bcl-2 expression level was decreased from 12 h. In contrast, the expression level of the proapoptotic protein Bax was increased very slightly until 48 h (Fig. 9c). Hence, as a result of these changes, the Bax to Bcl-2 and Bax to Bcl-xl ratios increased dramatically, reducing the integrity of the mitochondrial outer membrane. However, these events occurred after the loss of mitochondrial membrane potential, and combined with the results above, this timing indicates that although Bcl-2 family members play a crucial role in apoptosis induced by ruthenium(II) complexes, they appear to be synergistic factors rather than initiating factors in the process of apoptosis.

Conclusions

Six chiral ruthenium(II) complexes containing PIP derivatives were synthesized and characterized. Live-cell imaging and quantitative analysis by ICP-MS demonstrated that the ruthenium(II) complexes tended to accumulate preferentially in the mitochondria of HeLa cells. These ruthenium(II) complexes exhibited different inhibitory effects on cancer cells. Among these complexes, **Δ-Ru1** was found to have IC_{50} values relatively close to those of the well-known drug cisplatin for the cancer cell lines, and this complex was more cytotoxic to tumor cells than to normal cells. In addition, the cisplatin-resistant cell line A549-CP/R exhibited higher sensitivity to **Δ-Ru1** than to cisplatin. Further analysis showed that **Δ-Ru1** exerts its toxicity through the intrinsic mitochondria-mediated apoptotic pathway, which is accompanied by the regulation of Bcl-2 family members and the activation of caspases. Major challenges in cancer therapy are identifying and synthesizing drugs that kill tumor cells while preserving normal cells. Thus, **Δ-Ru1** may be a more potent and selective chemotherapeutic agent.

Acknowledgments This work was supported by the National Science of Foundation of China (nos. 21071155, 21172273, 21171177), the National High Technology Research and Development Program of China (863 Program, 2012AA020305), the National Science of Foundation of Guangdong Province (9351027501000003), the Research Fund for the Doctoral Program of Higher Education (20110171110013), the State Key Laboratory of Optoelectronic Materials and Technologies (2010-ZY-4-5), and Sun Yat-Sen University. X.H. thanks the Science and Technology Department of Hunan Province for support (2010FJ4090).

References

1. Rosenberg B, VanCamp L, Kriagas T (1965) Nature 205:698–699

2. Rosenberg B, VanCamp L, Trosko JE, Mansour VH (1969) Nature 222:385–386
3. Holmes J, Stanko J, Varchenko M, Ding H, Madden VJ, Bagnell CR, Wyrick SD, Chaney SG (1998) Toxicol Sci 46:342–351
4. Troy L, McFarland K, Littman-Power S, Kelly BJ, Walpole ET, Wyld D, Thomson D (2000) Psychooncology 9:29–39
5. Bruijnincx PC, Sadler PJ (2008) Curr Opin Chem Biol 12:197–206
6. Galanski M (2006) Recent Pat Anticancer Drug Discov 1:285–295
7. Kostova I (2006) Curr Med Chem 13:1085–1107
8. Bratsos I, Jedner S, Gianferrara T, Alessio E (2007) Chimia 61:692–697
9. Bergamo A, Sava G (2011) Dalton Trans 40:7817–7823
10. Hartinger CG, Jakupec MA, Zorbas-Seifried S, Groessl M, Egger A, Berger W, Zorbas H, Dyson PJ, Keppler BK (2005) Chem Biodivers 5:2140–2154
11. Sava G, Pacor S, Bergamo A, Cocchietto M, Mestroni G (1995) Chem Biol Interact 95:109–126
12. Jakupec MA, Arion VB, Kapitza S, Reisner E, Eichinger A, Pongratz M, Marian B, Keyserlingk NG, Keppler BK (2005) Int J Clin Pharmacol Ther 43:595–596
13. Liu HK, Sadler PJ (2011) Acc Chem Res 44:349–359
14. Gill MR, Derrat H, Smythe CGW, Battaglia G, Thomas JA (2011) ChemBioChem 12:877–880
15. Liu JG, Ye BH, Zhang QL, Zou XH, Zhen QX, Tian X, Ji LN (2000) J Biol Inorg Chem 5:119–128
16. Li LY, Jia HN, Yu HJ, Du KJ, Lin QT, Qiu KQ, Chao H, Ji LN (2013) J Inorg Biochem 113:31–39
17. Schatzschneider U, Niesel J, Ott I, Gust R, Alborzinia H, Wolfl S (2009) ChemMedChem 3:1104–1109
18. Chatterjee S, Kundu S, Bhattacharyya A, Hartinger C, Dyson P (2008) J Biol Inorg Chem 13:1149–1155
19. Meggers E (2007) Curr Opin Chem Biol 11:287–292
20. Du KJ, Wang JQ, Kou JF, Li GY, Wang LL, Chao H, Ji LN (2011) Eur J Med Chem 46:1056–1065
21. Kou JF, Qian C, Wang JQ, Chen X, Wang LL, Chao H, Ji LN (2012) J Biol Inorg Chem 17:81–96
22. Zhang PY, Wang JQ, Huang HY, Qiao LP, Ji LN, Chao H (2013) Dalton Trans 42:8907–8917
23. Yousif LF, Stewart KM, Kelley SO (2009) ChemBioChem 10:1939–1950
24. Gogvadze V, Orrenius S, Zhivotovsky B (2008) Trends Cell Biol 18:165–173
25. Kroemer G, Galluzzi L, Brenner C (2007) Physiol Rev 87:99–163
26. Fulda S, Galluzzi L, Kroemer G (2010) Nat Rev Drug Discov 9:447–464
27. Li L, Wong YS, Chen TF, Fan C, Zheng W (2012) Dalton Trans 41:1138–1141
28. Pierroz V, Joshi T, Leonidova A, Mari C, Schur J, Ott I, Spiccia L, Ferrari S, Gasser G (2012) J Am Chem Soc 134:20376–20387
29. Rodrigues FP, Pestana CR, Polizello ACM, Pardo-Andreu GL, Uyemura SA, Santos AC, Alberici LC, Silva RS, Curti C (2012) Nitric Oxide 26:174–181
30. Pisani MJ, Weber DK, Heimann K, Collins JG, Keene FR (2010) Metallomics 2:393–396
31. Ke HZ, Wang HD, Wong WK, Mak NK, Kwong DWJ, Wong KL, Tam HL (2010) Chem Commun 46:6678–6680
32. Pisani MJ, Fromm PD, Mulyana Y, Clarke RJ, Körner H, Heimann K, Collins JG, Keene FR (2011) ChemMedChem 6:848–858
33. Mulcahy SP, Gründler K, Frias C, Wagner L, Prokop A, Meggers E (2010) Dalton Trans 39:8177–8182
34. Chen TF, Liu YN, Zheng WJ, Liu J, Wong YS (2010) Inorg Chem 49:6366–6388
35. Yang XX, Chen LM, Liu YN, Yang YG, Chen TF, Zheng WJ, Liu J, He QY (2012) Biochimie 94:345–353
36. Chen TF, Mei WJ, Wong YS, Liu J, Liu YN, Xie HS, Zheng WJ (2010) MedChemComm 1:73–75
37. Yamada M, Tanaka Y, Yoshimato Y, Kuroda S, Shimao I (1992) Bull Chem Soc Jpn 65:1006–1011
38. Hua X, Zelewsky A (1995) Inorg Chem 34:5791–5797
39. Mosmann TJ (1983) Immunol Methods 65:55–63
40. Qian C, Wang JQ, Song CL, Wang LL, Ji LN, Chao H (2013) Metallomics 5:844–854
41. Elmes RPB, Orange KN, Cloonan SM, Williams DC, Gunnlaugsson T (2011) J Am Chem Soc 133:15862–15865
42. Zhang SJ, Hosaka M, Yoshihara T, Negishi K, Takeuchi T (2010) Cancer Res 70:4490–4498
43. Tian XH, Gill MR, Cantón I, Thomas JA, Battaglia G (2011) ChemBioChem 12:548–551
44. Ansari KI, Grant JD, Kasiri S, Woldemariam G, Shrestha B, Mandal SS (2009) J Inorg Biochem 103:818–826
45. Lecoeur H, Langonne A, Baux L, Rebouillat D, Rustin P, Prévost MC, Brenner C, Edelman L, Jacotot E (2004) Exp Cell Res 294:106–117
46. Xie CY, Zhu H, Lin LP, Miao ZH, Ding J (2007) Mol Cancer Ther 6:3059–3070
47. Meng XJ, Leyva ML, Jenny M, Gross I, Benosman S, Fricker B (2009) Cancer Res 69:5458–5466
48. Miura T, Tanno M, Sato T (2010) Cardiovasc Res 88:7–15
49. Vermes I, Haanen C, Nakken HS, Reutelingsperger C (1995) J Immunol Methods 184:39–51
50. Bhattacharjee RN, Park KS, Kumagai Y, Okada K, Yamamoto M, Uematsu S, Matsui K, Kumar H, Kawai T, Iida T, Honda T, Takeuchi O, Akira S (2006) J Biol Chem 281:36897–36904
51. Woldemariam GA, Mandal SS (2008) J Inorg Biochem 102:740–747
52. Ansari KI, Mishra BP, Mandal SS (2008) Biochim Biophys Acta 1779:66–73
53. Cai L, Li W, Wang GW, Guo LP, Jiang YC, Kang YJ (2002) Diabetes 51:1938–1948
54. Ames BN, Shigenaga MK, Hagen TM (1993) Proc Natl Acad Sci USA 90:7915–7922
55. Zafarullah M, Li WQ, Sylvester J, Ahmad M (2003) Cell Mol Life Sci 60:6–20
56. Tan CP, Wu SH, Wang M, Chen Y, Zhou L, Zhu Y, Lian W, Peng W, Ji L, Xu AL (2011) Dalton Trans 40:8611–8621
57. Gurp MV, Festjens N, Loo GV, Saelens X, Vandenabeele P (2003) Biochem Biophys Res Commun 304:487–497
58. Tan CP, Lai S, Wu SH, Hu S, Zhou L, Chen Y, Wang M, Zhu Y, Lian W, Peng W, Ji LN, Xu AL (2010) J Med Chem 53:7613–7624
59. Li P, Nijhawan D, Budihardjo I, Srinivasula SM, Ahmad M, Alnemri ES, Wang X (1997) Cell 91:479–489
60. Ly JD, Grubb DR, Lawen A (2003) Apoptosis 8:115–128
61. Green DR, Reed JC (1998) Science 281:1309–1312
62. Zhou HB, Aguilar A, Chen JF, Bai LC, Liu L, Meagher JL, Yang CY, McEachern D, Cong X, Jeanne A (2012) J Med Chem 55:6149–6161
63. Larsen AK, Escargueil AE, Skladanowski A (2003) Prog Cell Cycle Res 5:295–300
64. Tardito S, Barilli A, Bassanetti I, Tegoni M, Bussolati O, Gazzola RF, Mucchino C, Marchiò L (2012) J Med Chem 55:10448–10459
65. Willis S, Day CL, Hinds MG, Huang DCS (2003) J Cell Sci 116:4053–4056
66. Zhou J, Zhang S, Ong CN (2006) Biochem Pharmacol 72:132–136